DETERMINATION OF CRYSTALLINE, RIGID AMORPHOUS, AND MOBILE AMORPHOUS FRACTIONS IN ELECTROSPUN POLY(E-CAPROLACTONE) NANOFIBERS USING MODULATED DIFFERENTIAL SCANNING CALORIMETRY

László MÉSZÁROS[1,2], David LUKÁŠ[3], Roland PETRÉNY[1], Anna HLADÍKOVÁ[3], Kateřina BAADEROVÁ[3], Nina MAROUSKOVÁ[3], Balázs Gábor PINKE[1], Ema CHUDOBOVÁ[3], Jaroslav MIKULE[3], Eva KUŽELOVÁ KOŠŤÁKOVÁ[3]

[1]*Department of Polymer Engineering, Faculty of Mechanical Engineering, Budapest University of Technology and Economics, Műegyetem rkp. 3., H-1111 Budapest, Hungary, EU, meszaros.laszlo@gpk.bme.hu*

[2]*HUN-REN-BME Research Group for Composite Science and Technology, Budapest University of Technology and Economics, Műegyetem rkp. 3., H-1111 Budapest, Hungary, EU*

[3]*Technical University of Liberec, Studentská 2, 46117 Liberec, Czech Republic, EU, eva.kostakova@tul.cz*

https://doi.org/10.37904/nanocon.2025.5175

Abstract

Electrospun poly(ε-caprolactone) (PCL) nanofibers are promising materials for biomedical applications due to their biocompatibility and biodegradability. PCL is a semicrystalline polymer, and its functional properties are strongly influenced by its crystalline-amorphous morphology. While the crystalline and amorphous domains are commonly distinguished, recent studies on multiphase polymers suggest that the amorphous region can be further subdivided into rigid and mobile fractions. The so-called rigid amorphous phase (RAP) is typically located near the crystallite boundaries, where chain mobility is significantly restricted, while the mobile amorphous phase (MAP) retains high segmental mobility. In this study, we applied modulated differential scanning calorimetry (MDSC) to quantify the crystalline, RAP, and MAP fractions in electrospun PCL nanofibers. Although the three-phase model is known in filled polymers, i.e. polymers containing reinforcing or functional fillers, its application to nanofibrous systems has not been explored so far. Nanofibers were electrospun from 16 wt% PCL solution in chloroform:ethanol (8:2 wt), and multiple MDSC runs confirmed the reproducibility of phase separation. The crystalline fraction appeared as the most dominant phase, while both amorphous fractions were also clearly distinguishable. The phase proportions exhibited only minor variation across repeated measurements, supporting the robustness and reproducibility of the method. Since degradation behavior depends strongly on amorphous mobility, this approach may aid in designing resorbable nanofibrous scaffolds with tailored properties and controlled mechanical performance (e.g., tensile strength).

Keywords: Poly(ε-caprolactone; electrospun nanofibers; morphology; molecular mobility

1. INTRODUCTION

Poly(ε-caprolactone) (PCL) is a biodegradable polymer widely used in medical applications such as resorbable implants and drug-delivery systems. In these systems, the degradation rate is a key parameter, as it determines both the mechanical performance and the release kinetics of the active agent. The degradation behavior of PCL depends not only on the overall crystallinity but also on the internal morphology of the semicrystalline structure. Although the fiber diameter strongly affects the degradation rate through the available surface area, the internal organization of the crystalline and amorphous domains is also important [1-5].

The amorphous phase can be divided into two structurally distinct components: the rigid amorphous phase (RAP), where chain motion is restricted near crystalline interfaces, and the mobile amorphous phase (MAP),

where polymer segments retain higher mobility. The ratio of these two fractions can influence diffusion processes, moisture uptake, tensile properties, and the overall temporal profile of degradation. Differential scanning calorimetry (DSC), particularly in its modulated form, provides an effective means of quantifying the crystalline fraction and distinguishing between the RAP and MAP components [4, 6].

The present study compares the crystalline and amorphous phase composition of electrospun PCL nanofibers with that of the reference pellet, with special emphasis on the RAP/MAP balance and the reproducibility of the measured thermal response.

2. MATERIALS AND METHODS

2.1. Materials anf fiber preparation

The tested nanofibrous layer was produced by electrospinning from a polymer solution of polycaprolactone with a molecular weight of 45,000 g/mol (PCL45; Purasorb PC08, Corbion, Netherlands). The polymer concentration in the solution was 16 wt% and the solvent system consisted of chloroform and ethanol (Penta, Czech Republic) in a weight ratio of 8:2. The PCL pellet was also examined as a reference to reveal the effects of fiber formation on the resulting morphology. The polymer solution was spun using direct current (DC) continuous needle-less electrospinning, where the spinning-electrode is a static wire (NS 1S500U & NSAC150 Nanospider™ Production Line & Precisely controlled Air Conditioning Unit; Elmarco; Czech Republic). The following parameters were set for DC electrospinning: electrical potential difference between the spinning electrode and the collector 50 kV; distance between the spinning electrode and the collector 180 mm; temperature 22±1 °C; relative humidity 30±2 %, withdrawal speed of the substrate fabric 48 mm/min; substrate fabric polypropylene spunbond with an area weight of 30 g/m^2 (PFNonwovens; Czech Republic).

2.2. Modulated differential scanning calorimetry

The thermal transitions of the PCL nanofibers was analysed by modulated differential scanning calorimetry (MDSC) using a DSC Q2000 instrument equipped with an RCS (90) cooling unit (TA Instruments, New Castle, DE, USA). Approximately 10 mg of each sample was sealed in standard aluminium pans and measured under a nitrogen purge of 50 ml min^{-1}. Before heating, the specimens were equilibrated at –90 °C for 5 min to ensure thermal stabilization. A temperature modulation of ±1 °C with a 60 s period was applied during a single linear heating ramp of 5 °C min^{-1} up to 100 °C. The measurement was repeated five times to assess repeatability.

2.3. Scanning electron microscopy (SEM) and fiber diameter distribution

The electrospun PCL nanofibers were examined using a JEOL JSM-6380LA scanning electron microscope (JEOL Ltd., Japan). Prior to observation, the samples were sputter-coated with a thin gold layer to ensure electrical conductivity. Micrographs of the electrospun mats were taken at various magnifications for the subsequent evaluation of fiber diameters.

The resulting nanofibrous layer had an areal weight of 20±1 g/m^2. Images from the scanning electron microscope and the ImageJ Fiji image processing package were used to analyse fiber diameters. The measured diameters were grouped into size classes, and the number of fibers in each class was plotted to obtain a fiber-diameter histogram. To better represent the relative mass contribution of fibers of different diameters, the data were further processed to construct a mass-weighted distribution. Assuming cylindrical fibers of uniform density and effectively infinite length (as no fiber ends were visible in the SEM micrographs), the mass fraction of each diameter class, w_i, was calculated as

$$w_i = \frac{n_i d_i^2}{\sum_j n_j d_j^2}, \quad (1)$$

where n_i is the number of fibers in the given class and d_i is the class-midpoint diameter. The denominator represents the total fiber mass estimated from all classes. This representation better reflects the contribution of thicker fibers to the overall mass and was therefore used for correlation with the DSC results.

2.4. Determination of glass transition temperature

The glass transition temperature of PCL was determined from the total heat-flow curve obtained during the heating scan. Linear baselines were fitted to the pre- and post-transition regions, and the intersection points were used to calculate the onset, midpoint, and endset temperatures according to the midpoint method implemented in the TA Universal Analysis software.

2.5. Determination of the degree of crystallinity (X_c)

The degree of crystallinity was determined by integrating the melting endotherm of the total heat flow curve. The X_c was calculated as [4]

$$X_c\ (\%) = \frac{\Delta H_m}{\Delta H_0} \cdot 100 \quad (2)$$

where ΔH_m – the measured crystal melting enthalpy change; ΔH_0 – the crystal melting enthalpy change at a 100% crystalline phase ratio, which is 139.5 J/g for PCL [1]. The integration was performed using the Integrate peak (linear baseline) function of the TA Universal Analysis software within the temperature range of 25–75 °C, corresponding to the entire melting region of the polymer. The melting temperature (T_m) was taken as the temperature of the peak maximum.

2.6. Determination of the mobile and rigid amorphous phases

The reversible specific-heat-capacity change at the glass transition ($\Delta c_{p,rev}$) was evaluated from the reversible heat-flow signal of the heating scan using the TA Universal Analysis software by fitting linear baselines to the pre- and post-transition regions of the reversible heat-flow curve and taking the difference of these baselines at the midpoint temperature of the transition step. The mobile amorphous fraction (MAP) was calculated as [4]

$$MAP\ (\%) = \frac{\Delta c_{p,\ rev}^{sample}}{\Delta c_{p,\ rev}^{amorphous\ reference}} \cdot 100 \quad (3)$$

where $\Delta c_{p,\ rev}^{amorphous\ reference}$ is the reversible heat-capacity increment of a fully amorphous reference of PCL (0.59 J/(g°C) [7]). The rigid amorphous phase (RAP) was determined by

$$RAP\ (\%) = 100 - MAP - X_c, \quad (4)$$

where X_c is the crystalline mass fraction obtained from the melting enthalpy.

3. RESULTS AND DISCUSSION

The base fibrous PCL structure consisted of a mixture of smooth, uniform, and bead-free fibers, including thick and thin fibers, as well as significantly finer fibers that frequently bridged the gaps between the larger ones (see **Figure 1a and b**). The measured average fiber diameter was 573 nm (standard deviation 728 nm; 95% confidence interval 100 nm). The diameter histogram (**Figure 1c**) shows a wide distribution dominated by fine fibers but extending toward micrometer-scale diameters. Most fibers had diameters below 600 nm, while a smaller population of thicker fibers extended up to several micrometers. When the same data were expressed as a mass-weighted distribution (**Figure 1d**), the relative importance of the thicker fibers increased considerably, indicating that despite their smaller number, they contribute significantly to the total mass of the

fibrous mat. This dual representation highlights the heterogeneous nature of the structure and confirms the coexistence of fine and thicker fibers within the PCL network.

Figure 2 shows the total heat-flow curves recorded during the heating of the nanofiber mat (black curve) and the reference pellet (red curve), revealing the glass transition and the subsequent melting process. Evaluation of the total heat-flow curve of the nanofibers yielded a glass-transition temperature (T_g) of –62.8 ± 0.7 °C, indicating that the amorphous phase exhibits normal chain mobility. The relatively low standard deviation confirms excellent repeatability and thermal homogeneity among the samples. The T_g of the nanofibers showed no significant difference from that of the reference pellet (–63.3 °C).

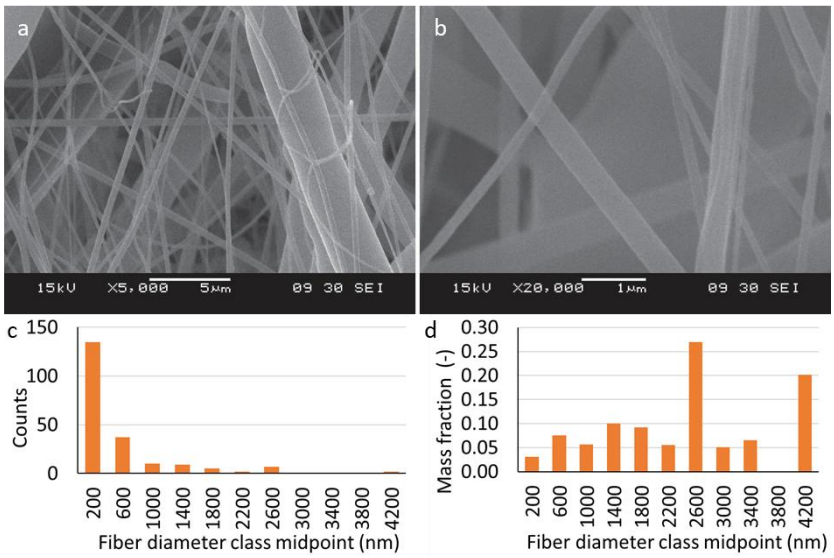

Figure 1 Representative SEM micrographs of the electrospun PCL nanofibers recorded at (a) 5000× and (b) 20 000× magnifications. The corresponding fiber-diameter data are presented as (c) the number of counted fibers in each diameter class and (d) the calculated mass-weighted distribution.

The melting endotherm of PCL exhibited a pronounced shoulder – as indicated by the blue arrow in **Figure 2** – preceding the main melting peak, very similar in shape to that reported by Tenorio-Alfonso et al., [8]. In that study, the lower-temperature shoulder was attributed to the melting of thinner and less perfect lamellae, or crystallites that reorganize upon heating before melting at higher temperatures. We therefore ascribe the shoulder observed in our samples to the presence of such less perfect lamellar populations.

As can be clearly seen in **Figure 2**, the melting curve of the nanofiber mat is shifted towards lower temperatures compared to that of the reference pellet, as indicated by the green arrow. The main melting peak appeared at 59.3 ± 0.2 °C, while that of the pellet was observed at 62.3 °C, confirming a distinct and remarkable shift of the melting region towards lower temperatures. The exceptionally low standard deviation of the melting temperature of the nanofibers further supports the reliability of this observation, demonstrating that the measured behavior is highly reproducible despite the inherent porosity and preparation challenges of electrospun mats. The decrease in T_m can be attributed to the confinement imposed by the nanofibrous morphology. The restricted space available for crystal growth and lamellar thickening results in the formation of thinner and less perfect lamellae with reduced thermal stability. According to the Gibbs–Thomson principle [9], such thinner lamellae melt at lower temperatures due to their higher surface free energy. The coexistence of these less perfect crystallites with the more stable lamellae gives rise to the shoulder observed on the low-temperature side of the melting endotherm. This behavior is consistent with the large number of thin nanofibers present in the mat, where the limited space available for crystal thickening likely promotes the formation of smaller and less perfect crystallites. Although these thinner fibers are numerous, the majority of the melting enthalpy originates from the melting of thicker fibers, which dominate the mass-weighted contribution to the

melting endotherm. Overall, the melting behavior reflects a heterogeneous lamellar population characteristic of electrospun PCL, combining the effects of confinement and non-equilibrium crystallization during fiber formation. The degree of crystallinity was 62.0 ± 1.1%. The low standard deviation demonstrates the excellent repeatability of the measurement and indicates that the characteristic heterogeneous crystalline structure developed consistently throughout the produced fibrous mat. The crystallinity level is practically identical to that of the reference pellet (60.9%), showing that the electrospinning process had no significant effect on the overall degree of crystallinity.

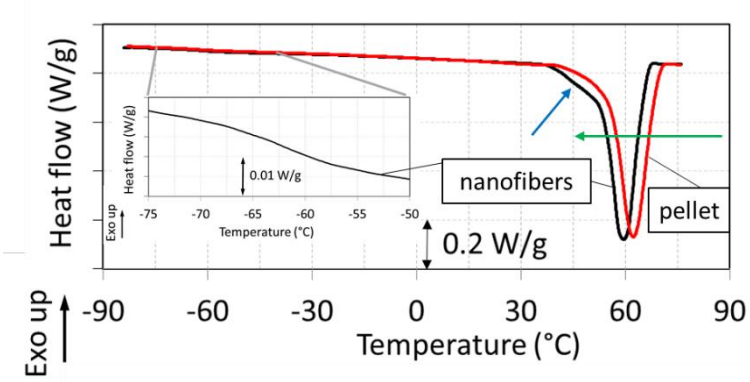

Figure 2 Heat flow curves of poly(ε-caprolactone) (PCL) nanofibers and the reference pellet. The inset shows an enlarged section of the curve to make the glass transition region more clearly visible.

The presence of a well-defined main melting peak further confirms the existence of extended crystalline regions within the fibers. As discussed above for the melting shoulder, this interpretation is consistent with the fiber diameter distribution: thinner fibers are more likely to contain imperfect crystallites, whereas the thicker ones – representing the main fraction of the sample mass – dominate the distinct melting peak. Overall, these results show that the nanofibrous geometry, while limiting lamellar thickening and introducing some heterogeneity in lamellar perfection, still allowed for efficient crystallization under the applied processing conditions.

The ratio of the rigid amorphous phase (RAP) to the mobile amorphous phase (MAP) reflects the degree of chain immobilization at crystalline–amorphous interfaces. In the electrospun nanofibers (Figure 3 a), the RAP fraction (15.9%) was significantly lower, while the MAP fraction (22.1%) was higher compared to the reference pellet (**Figure 3b**; RAP = 28.4%, MAP = 10.7%).

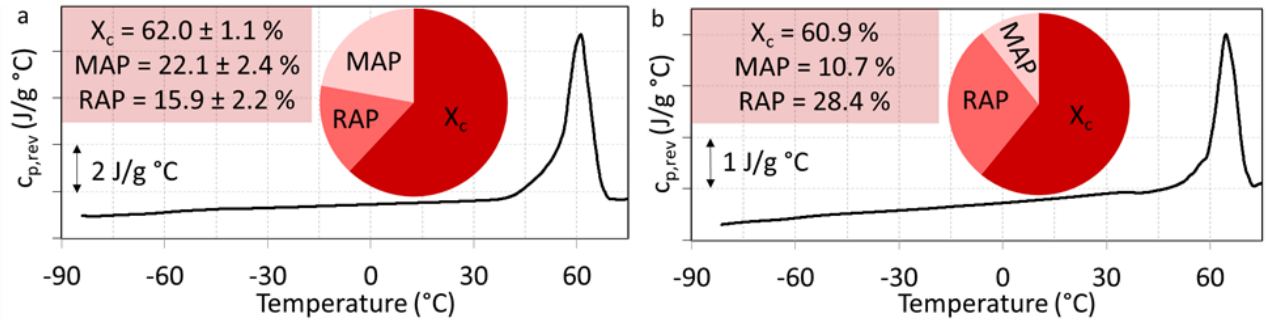

Figure 3 Reversing specific heat-capacity curves ($c_{p,rev}$) of (a) electrospun PCL nanofibers and (b) the reference pellet. The inset pie charts show the relative fractions of the crystalline (X_c), rigid amorphous (RAP), and mobile amorphous (MAP) phases.

This difference means that the amorphous regions in the nanofibers contain chain segments with substantially higher mobility compared to the pellet. Such increased mobility may result from the presence of smaller and

less perfect crystallites, which impose weaker constraints on the neighboring amorphous chains. In nanofibers, crystal growth is expected to proceed predominantly in the radial direction. However, surface effects at the fiber boundary can disturb the regular packing of chains, leading to the formation of thinner and less perfect lamellae. The smaller the fiber diameter, the higher the specific surface area, and consequently, the stronger the influence of surface-related phenomena, which tend to hinder regular crystallization near the fiber surface. As a result, the overall crystallinity remains comparable to the bulk material, but the lamellar morphology becomes less ideal and thermally less stable.Consequently, the higher MAP fraction provides additional chain flexibility and may contribute to enhanced relaxation capability and ductility of the nanofibrous mat.

4. CONCLUSION

Differential scanning calorimetry revealed clear structural differences between electrospun PCL nanofibers and the reference pellet. The nanofibers showed a slight reduction in melting temperature and the presence of less perfect crystallites, reflecting the confinement and non-equilibrium conditions during fiber formation. These effects are consistent with the broad diameter distribution of the electrospun fibers, where thinner fibers are more prone to structural imperfections. Nevertheless, the overall crystallinity remained comparable to that of the bulk material, confirming that electrospinning did not markedly suppress crystallization.

In the nanofibers, the higher fraction of the mobile amorphous phase indicates increased molecular mobility within the amorphous regions, which may facilitate water penetration and accelerate degradation in biomedical applications. The high reproducibility of the thermal parameters confirms the structural homogeneity of the electrospun mats and the reliability of the applied characterization approach.

ACKNOWLEDGEMENTS

This work was supported by the Hungarian State Eötvös Scholarship, funded by the Ministry of Culture and Innovation (KIM), Hungary, and administered by the Tempus Public Foundation. The research was also supported by Czech Science Foundation Grant No. 23-05154S Investigation of prokaryotic and eukaryotic cell interactions with nanofibers differing in morphology and structure.

REFERENCES

[1] A. FERNÁNDEZ-TENA *et al.*, “Effect of Molecular Weight on the Crystallization and Melt Memory of Poly(ε-caprolactone) (PCL),” *Macromolecules*. Vol. 56, no. 12, pp. 4602–4620, June 2023. Available from: https://doi.org/10.1021/acs.macromol.3c00234.

[2] J. R. DIAS, A. SOUSA, A. AUGUSTO, P. J. BÁRTOLO, and P. L. GRANJA. “Electrospun Polycaprolactone (PCL) Degradation: An In Vitro and In Vivo Study.” *Polymers (Basel)*. Vol. 14, no. 16, p. 3397, Aug. 2022. Available from: https://doi.org/10.3390/polym14163397.

[3] C.-S. WU, S.-S. WANG, D.-Y. WU, and W. GU. “Modified poly(ε-caprolactone) with larvae protein environmentally friendly nanofiber: Assessment of interface properties and characterization.” *Express Polym. Lett.*. Vol. 18, no. 8, pp. 835–850, 2024. Available from: https://doi.org/10.3144/expresspolymlett.2024.62.

[4] L. MÉSZÁROS, Á. BEZERÉDI, and R. PETRÉNY, “Modifying the properties of polyamide 6 with high-performance environmentally friendly nano- and microsized reinforcing materials.” *Polymer Composites*. Vol. 45, no. 7, pp. 6404–6413, 2024. Available from: https://doi.org/10.1002/pc.28205.

[5] M. MUSIOŁ, J. RYDZ, W. SIKORSKA, H. JANECZEK, and S. JURCZYK. “Organic recycling challenges of (bio)degradable packages: Degradation studies of polylactide/cork composites.” *Express Polym. Lett.* Vol. 18, no. 8, pp. 868–880, 2024, Available from: https://doi.org/10.3144/expresspolymlett.2024.64.

[6] W. LIMSUKON, M. RUBINO, M. RABNAWAZ, L.-T. LIM, and R. AURAS. “Hydrolytic degradation of poly(lactic acid): Unraveling correlations between temperature and the three phase structures.” *Polymer Degradation and Stability*. Vol. 217, p. 110537, Nov. 2023. Available from: https://doi.org/10.1016/j.polymdegradstab.2023.110537.

[7] R. SABATER I SERRA, A. KYRITSIS, J. L. ESCOBAR IVIRICO, J. L. GÓMEZ RIBELLES, P. PISSIS, and M. SALMERÓN-SÁNCHEZ. “ Molecular mobility in biodegradable poly(-caprolactone)/poly(hydroxyethyl acrylate) networks. *Eur. Phys. J. E*. Vol. 34, no. 4, p. 37, Apr. 2011. Available from: https://doi.org/10.1140/epje/i2011-11037-4.

[8] A. TENORIO-ALFONSO, E. VÁZQUEZ RAMOS, I. MARTÍNEZ, M. AMBROSI, and M. RAUDINO. “Assessment of the structures contribution (crystalline and mesophases) and mechanical properties of polycaprolactone/pluronic blends.” *Journal of the Mechanical Behavior of Biomedical Materials*. Vol. 139, p. 105668, Mar. 2023. Available from: https://doi.org/10.1016/j.jmbbm.2023.105668.

[9] X. YU, N. WANG, and S. LV. “Crystal and multiple melting behaviors of PCL lamellae in ultrathin films.” *Journal of Crystal Growth*. Vol. 438, pp. 11–18, Mar. 2016. Available from: https://doi.org/10.1016/j.jcrysgro.2015.12.021.